Eur. Phys. J. Special Topics **222**, 2119–2142 (2013)

DOI: 10.1140/epjst/e2013-01990-0

THE EUROPEAN PHYSICAL JOURNAL SPECIAL TOPICS

Review

Spectral line-shapes investigation with Pound-Drever-Hall-locked frequency-stabilized cavity ring-down spectroscopy

A. Cygan[1], S. Wójtewicz[1], J. Domysławska[1], P. Masłowski[1], K. Bielska[1], M. Piwiński[1], K. Stec[1], R.S. Trawiński[1], F. Ozimek[3], C. Radzewicz[3], H. Abe[4], T. Ido[5], J.T. Hodges[2], D. Lisak[1], and R. Ciuryło[1,a]

[1] Institute of Physics, Faculty of Physics, Astronomy and Informatics, Nicolaus Copernicus University, Grudziadzka 5, 87-100 Torun, Poland
[2] National Institute of Standards and Technology, 100 Bureau Drive, Gaithersburg, Maryland 20899, USA
[3] Instytut Fizyki Doświadczalnej, Wydział Fizyki, Uniwersytet Warszawski, Hoża 69, 00-681 Warszawa, Poland
[4] National Metrology Institute of Japan (NMIJ), AIST, Tsukuba Central 3, Tsukuba 305-8563, Japan
[5] National Institute of Information and Communications Technology, Koganei, Tokyo 184-8795, Japan

Received 8 June 2013 / Received in final form 9 August 2013
Published online 23 October 2013

Abstract. A review of recent experiments involving a newly developed Pound-Drever-Hall-locked frequency-stabilized cavity ring-down spectroscopy (PDH-locked FS-CRDS) system is presented. By comparison to standard FS-CRDS, the PDH lock of the probe laser to the ring-down cavity optimized coupling into the cavity, thus increasing the ring-down signal acquisition rate nearly 300-fold to 14 kHz and reducing the noise-equivalent absorption coefficient by more than an order of magnitude to 7×10^{-11} cm^{-1}. We discuss how averaging approximately 1000 spectra yielded a signal-to-noise ratio of 220000. We also discuss how the spectrum frequency axis was linked to an optical frequency comb, thus enabling absolute frequency measurements of molecular optical transitions at sub-MHz levels. Applications of the spectrometer to molecular line-shape studies are also presented. For these investigations, we use semi-classical line-shape models that consider the influence of Dicke narrowing as well as the speed dependence of the pressure broadening and shifting to fit spectra. We show that the improved precision and spectrum fidelity of the spectrometer enable precise determinations of line-shape parameters. We also discuss the importance of line-shape analysis with regard to the development of new spectroscopic databases as well as in the optical determination of the Boltzmann constant.

[a] e-mail: rciurylo@fizyka.umk.pl

1 Introduction

Recently, a more fundamental understanding of atomic and molecular line shapes has led to tremendous progress in diverse fields of physical research. For example, accurate data on line-shape parameters and intensities are the basis for the development of modern Earth and planetary atmospheric monitoring systems. The Fourier-transform spectrometers mounted on satellite-borne instruments are being designed to collect spectroscopic data with a relative precision better than 0.5% [1], allowing the investigation of small spatial and temporal fluctuations in the concentration and flux of measured gas species [2]. However, the use of accurate reference line-shape parameters is a key to exploiting the full precision of these devices in the analysis of atmospheric spectra. Such laboratory data, which are characterized by standard uncertainties at the sub-percent level, will be used in the future generations of spectroscopic databases. Precise and accurate metrology of gas volume and its composition is important for chemical substance studies, human breath analysis [3,4] and semiconductor manufacturing processes [5]. The spectroscopy of trace gas detection and careful line-shape examination are especially relevant to the last two cases. Advances in high-resolution spectroscopic techniques have enabled more stringent tests of theoretical line-shape models [6–15], verification of atomic and molecular interaction potentials [16–22], detection of isotopic composition [23–26] and deconvolution of hyperfine spectra [27]. Recent work on optical determination of the Boltzmann constant [28–32] requires experimental conditions that give exceptional precision and accuracy at the 10^{-6} level or below. In order to obtain such accuracy in the measured Doppler width, measured spectra must be described by the correct line-shape model [33–36]. Atomic frequency standards that are commonly used for laser frequency stabilization and as absolute frequency references for measured spectra [37–40] are another example where sophisticated line-shape studies are required.

Advances in experimental methods have been successfully realized in recent years especially with regard to performance metrics such as sensitivity, precision and accuracy, spectral resolution, and frequency stability. High sensitivity measurements of weak atomic and molecular transitions essential for the remote sensing and medical purposes were demonstrated both by photo-acoustic [41–43] as well as indirect absorption techniques such as laser-induced fluorescence [44]. However, only direct absorption spectroscopy with the use of optical cavities offers the combination of frequency resolution, sensitivity and absolute absorption scales without the need to calibrate in terms of a reference absorption standard. The lowest detection limits of $1 \times 10^{-14}\,\mathrm{cm}^{-1}\mathrm{Hz}^{-1/2}$ and $1 \times 10^{-12}\,\mathrm{cm}^{-1}\mathrm{Hz}^{-1/2}$ achieved in cavity-enhanced experiments were demonstrated by Ye, Ma and Hall [45] with the NICE-OHMS technique and by Spence et al. [46] with cavity ring-down spectroscopy (CRDS) assisted by the Pound-Drever-Hall (PDH) [47], respectively. More recently, there has been a dramatic increase in the spectrum signal-to-noise ratios (SNR) relative to those typically obtained in line-shape studies (which were of the order 1000–2000). Measurements reporting SNRs of the order of 28000 [48], 100000 [49] or even 200000 [50] have become possible in optical, terahertz and microwave absorption spectroscopy, respectively.

Progress in the construction of ultra-stable lasers characterized by line widths smaller than 40 mHz, was demonstrated recently by PTB and JILA groups [51]. This capability opens new paths toward the development of short-term optical frequency standards for optical atomic clocks and ultra-high-resolution spectroscopy that are required for advanced studies of new physical effects and studies of the stability of physical constants [52–54].

The development of the self-referenced optical frequency comb (OFC) [55,56] enabled relatively simple but precise and highly accurate measurements of optical frequencies. OFCs have found numerous applications in variety of research fields [57,58].

The broadband spectrum of a femtosecond laser can be matched to the spectrum of resonances of an enhancement cavity and used directly for interrogation of molecular samples [59–63], allowing real-time simultaneous measurements in thousands of channels with sensitivity limited only by quantum noise [64,65].

In this review, we describe the development of the optical frequency comb-assisted Pound-Drever-Hall-locked frequency-stabilized cavity ring-down spectroscopy method (PDH-locked FS-CRDS) [66–70]. This approach combines high precision and accuracy in the absorption axis, with high resolution and stability in the spectrum frequency axis. The PDH-locked FS-CRDS technique is a natural consequence and extension of FS-CRDS, which was developed and originally applied in 2004 to molecular line-shape studies by Hodges and coworkers [71,72] at the National Institute of Standards and Technology (NIST). Herein, we show how our improvements to the FS-CRDS technique have enabled ultra-high-SNR spectral line-shape measurements that can be placed on an absolute frequency axis. This work has resulted in the most accurate data on O_2 B-band line shapes reported in the literature [21,73] and an extremely high SNR of 220000 [74] which to the best of our knowledge is the highest one ever obtained in the optical domain. We discuss here the benefits of using a multi-spectrum fit procedure [75] to disentangle line-shape parameters that are correlated over a range of pressure. We indicate that the instrument described here can provide data for spectroscopic data bases with a relative uncertainty less than 1%. This also requires the use of line-shape models that are more sophisticated than the Voigt profile.

2 Line-shape theory

A proper description of molecular line shapes under atmospheric conditions requires that several effects be considered [76,77]. Of these mechanisms, the most well-known are Doppler broadening and collisional broadening and shifting. The Voigt profile, which is a convolution of the Gaussian and Lorentz distributions, accounts for both of these effects. This profile is obtained assuming that the Doppler broadening (described by the Gaussian distribution) is statistically independent of the collisional broadening and shifting (described by the Lorentz distribution). Moreover, it is assumed that the motion of the absorber is unperturbed by collisions, and the collisional broadening and shifting are independent of absorber speed and can be described in the framework of the impact approximation [78,79].

A few decades ago it was realized that Doppler broadening can be significantly reduced by velocity-changing collisions that lead to the so-called Dicke narrowing [80,81]. In order to model this effect, the Galatry profile (GP) [82] and Nelkin-Ghatak profile (NGP) [83] were derived and based on the soft (weak) and hard (strong) collision models, respectively [84–86]. Subsequently, the Rautian-Sobelman profile (RSP) [84,85] and the Keilson-Storer profile (KSP) [87,88] were developed to account for a smooth transition between the soft and hard collision models. All of these models neglect the dependence of the frequency of velocity-changing collisions on the velocity of the absorbing molecule. The hard collision model was generalized to the case of the velocity-dependent collision frequency in Ref. [89] using the so-called kangaroo model. To get a more realistic description of the velocity-changing collisions it is necessary to resort to analytical expressions that describe the shape of the spectral line and calculate the line profile numerically by solving appropriate transport/relaxation equations [88,90–92]. This approach, which was explored by Blackmore [90] and others [93], leads to the billiard-ball profile (BBP) with the velocity-changing collisions described by collisions of hard spheres. The BBP model applied in the absence of collisional broadening and shifting is equivalent to the self-structure factor evaluated earlier by Lindenfeld [94]. The use of hard-sphere collision models allows one to

naturally account for the dependence of the frequency of the velocity-changing collisions on the absorber velocity as well as the fraction of velocity-changing collisions on the perturber-to-absorber mass ratio β. An alternative approach that gives similar information and also leads to a realistic description of the velocity-changing collisions is based on molecular dynamic simulations. Hoang et al. [95] and Joubert et al. [96] first used this technique to estimate and interpret parameters of analytical kernels [97–99] which describe the velocity-changing collisions that determine the shape of the spectral line.

In principle, the Dicke narrowing is related to the mean free path of an absorbing molecule. It is convenient to define the effective frequency of velocity-changing collisions ν_{diff} which can be related to the mass diffusion coefficient D by: $\nu_{\text{diff}} = k_B T/(mD)$ [80,100], where k_B is the Boltzmann constant, T is temperature and m is the absorber mass. Usually the same collisions that lead to changes in the absorber velocity also cause a phase shift in the absorbed radiation or can lead to change of the absorber quantum state. The main influence of the dephasing and state-changing collisions on the spectral line shape in the low-pressure regime is manifest as collisional broadening and shifting. Nevertheless, the inherent correlation between velocity-changing and dephasing and/or state-changing collisions also affects the magnitude of the Dicke narrowing [84,85,101–103]. In most common cases where these correlations play some role [104,105], it is useful to introduce an optical frequency of velocity-changing collisions ν_{opt} which in general can be complex as first proposed by Rautian and Sobelmann [84,85]. The occurrence of a complex narrowing parameter leads to the line-shape asymmetry, which was observed and interpreted in these terms by Pine [106]. See also Ref. [107]. Several attempts to estimate the magnitude of ν_{opt} were performed using the semi-classical approach [108,109], quantum scattering calculations [110] and molecular dynamic simulations [111,112].

In many cases, collisional broadening and shifting cannot be treated as being independent of the absorber speed. More generally, the speed dependence of the collisional broadening and shifting is caused by the absorber-perturber interaction and depends on β. This effect is negligible when β approaches zero and becomes more important with increasing β. Berman [113] first noted this problem and derived the speed-dependent Voigt profile (SDVP), which takes into account both the Doppler broadening and the speed-dependent collisional broadening and shifting. Line-shape theory predicts that speed dependence of the collisional broadening can lead to a narrower line shape than in the speed-independent case [113,114]. On the other hand, the speed-dependent collisional shift can lead to some line asymmetry [113,114]. In the case where the Doppler broadening can be neglected, in the so-called collision regime, Pickett [115] introduced a weighted sum of Lorentz profiles (WSLP). It can be shown that in some specific cases, like in the case of H_2 lines perturbed by Ar [116], where the strongly speed-dependent collisional shifting is much bigger than the collisional broadening, the speed-dependent profile can be wider than the speed-independent one. All of these predicted features of speed-dependent profiles have been confirmed by early laser experiments in atomic and molecular systems [116,117].

Quite early it was shown by Ritter and Wilkerson [118] that in the case of a typical molecular transition, where collisional broadening often is significantly bigger than collisional shifting, it is difficult to definitively identify the physical origin of the observed line narrowing and deviations from the Voigt profile. More specifically, it is often difficult to distinguish between Dicke narrowing and the speed dependence of the collisional broadening. This problem was addressed in detail by Rohart and his collaborators [119] as well as by others [20,120,121].

Duggan et al. [122] showed that the analysis of measured molecular line shapes requires profiles that account for both effects: Dicke narrowing and the speed dependence of the collisional broadening and shifting. See also Ref. [123]. They did

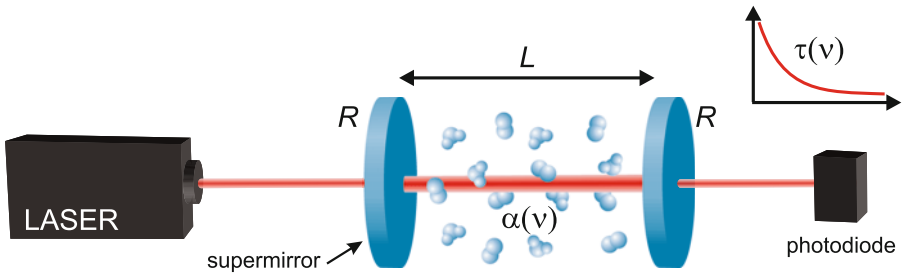

Fig. 1. Scheme of cavity ring-down spectroscopy experimental setup.

this analysis using a convolution of the GP and WSLP profiles. In the framework of the soft- and hard-collision models, the speed-dependent Galatry profile (SDGP) [124,125] and speed-dependent Nelkin-Ghatak profile (SDNGP) [126] have been given. These speed-dependent profiles can be easily combined using the Rautian-Sobelman model of velocity-changing collisions [84,85] as shown in Refs. [127–129]. This approach also allows one to include the possible correlation between velocity-changing and dephasing and/or state-changing collisions as well as dispersion asymmetry of the line. A profile that includes all of these effects is called the correlated speed-dependent asymmetric Rautian-Sobelman profile (CSDARSP) [129,130]. Assuming only hard velocity-changing collisions and neglecting the dispersion asymmetry, this profile can be reduced to the correlated speed-dependent Nelkin-Ghatak profile (CSDNGP) introduced by Pine [17], which is comparatively easy to use.

Speed-dependent line shapes can be modeled even more realistically with velocity-changing collisions that are described by collisions of hard spheres [94] or molecules that interact according to an inverse-power potential [90]. Properties of such models were discussed in detail for the speed-dependent billiard-ball profile (SDBBP) [93] and the speed-dependent Blackmore profile [131,132]. Again, the correlation between velocity-changing and dephasing and/or state-changing collisions as well as the dispersion asymmetry of the line can be incorporated into these models [133]. The correlated speed-dependent billiard-ball profile (CSDBBP) in which ν_{opt} is used in place of ν_{diff} was first applied by Wehr et al. [20,134] for interpretation of molecular line shapes and was described in detail in Ref. [11].

An ultimate goal for line-shape theory is to base the calculations on fundamental physical principles, thus avoiding the simplifications used to derive the models described above. At present, there are two ways of doing *ab initio* calculations of this type. The first is to solve the proper transport/relaxation equation as demonstrated by Blackmore et al. [135] and reviewed by May et al. [92], and the second way, recently developed by Hartmann et al. [14,15] is based on molecular dynamics simulations.

3 Cavity ring-down spectroscopy technique

In the simplest version of cavity ring-down spectroscopy, a gaseous sample is placed between two mirrors that form a high-finesse optical resonator (Fig. 1) [136–138]. This arrangement yields effective optical path lengths up to hundreds of kilometers, thus enabling the measurement of extremely low intensity spectra and strong absorbers at trace concentrations. CRDS yields the absorption coefficient $\alpha(\nu)$ in terms of the measured decay time constant $\tau(\nu)$, which is associated with the rate at which light intensity leaks out of the cavity [138]:

$$\tau(\nu) = \frac{L}{c(1 - R + \alpha(\nu)L)}, \tag{1}$$

where L is the mirror-to-mirror distance, R is the geometric-mean intensity reflectivity of the high-reflectivity mirrors (supermirrors) comprising the resonator and c is the speed of light. An important advantage of the CRDS technique is its insensitivity to fluctuations in probe laser power and to stray light in the laboratory. The single-shot detection limit $\Delta\alpha$ in CRDS experiments can be reduced by extending τ and/or by reduction of its measurement uncertainty σ_τ, according to the relation:

$$\Delta\alpha = \frac{1}{c\langle\tau\rangle}\frac{\sigma_\tau}{\langle\tau\rangle}, \tag{2}$$

where $\sigma_\tau/\langle\tau\rangle$ and $\langle\tau\rangle$ are the relative standard deviation and mean value, respectively, of τ. Assuming a Gaussian distribution of measured τ values, the statistical noise σ_τ can be decreased by averaging k decay signals according to the formula $\sigma_\tau/\sqrt{k}$.

The earliest reports of cavity-enhanced absorption measurements for a gaseous medium placed within a Fabry-Pérot interferometer, date from the early 1960's [139,140]. In 1974 Kastler [141] was the first to measure the exponential decay of light leaking from a low-finesse optical cavity. In the course of developing mirrors of extremely high reflectivity (i.e. $R = 99.999\%$) various techniques for measuring mirror τ were implemented. The first technique, proposed by Herbelin et al. [142] in 1980, was to determine τ from measurements of the phase delay of amplitude-modulated light passing through a resonant cavity. In 1984 Anderson et al. revisited Kastler's idea and determined τ by direct observation of the exponential decay of light exiting the cavity [143]. During the next four years Anderson's technique was improved in the context of increases in cw-laser-to-cavity coincidences by placing one of the cavity mirrors on a piezo-electric transducer (PZT) and by scanning the cavity length [144]. In 1988 O'Keefe and Deacon were the first to demonstrate gas phase absorption in the cavity medium by measuring τ. Their experiment involved absorption measurements of weak B ($b^1\Sigma_g^+(\nu = 1) \leftarrow X^3\Sigma_g^-(\nu = 0)$, around 689 nm) and Γ ($b^1\Sigma_g^+(\nu = 2) \leftarrow X^3\Sigma_g^-(\nu = 0)$, around 628 nm) bands of the O_2 [145]. At this moment a new type of absorption spectroscopy, named *cavity ring-down spectroscopy*, was born.

The first realizations of CRDS involved pulsed laser sources which yielded sufficient bandwidth to ensure spectral overlap of the probe laser and cavity resonances. However, excitation of multiple transverse and longitudinal cavity modes lead to mode beating and consequently to multi-exponential decays. In 1996 Hodges, Looney and van Zee [146] considered the influence of pulsed laser bandwidth on CRDS spectrum fidelity followed by a theoretical model [147]. Three years later this group [148] demonstrated the first pulsed-CRDS experiment with single-mode excitation resulting in single exponential decays, in which a relative precision in τ equal to 0.03% was achieved.

Continuous-wave (cw) lasers were introduced to the high resolution gas phase CRDS spectroscopy by Romanini et al. [149] in 1997, as proposed by Lehmann [150,151]. However, ten years earlier, Curran et al. [152] used cw-lasers to detect absorption in a thin layer on a mirror surface. The comparison of pulsed- and cw-CRDS techniques, presented in [148], clearly indicated a noticeable improvement of the measurement detection limits afforded by the latter method down to 10^{-9}–10^{-10} cm^{-1}. In cw-CRDS with narrowband lasers, spectral overlap of the probe laser and cavity resonances must be realized, and this can be achieved in two ways - by changing the cavity length or by tuning the laser frequency. Further, in order to acquire an exponentially decaying ring-down signal, the turn-off time of the probe laser beam must be much less than the cavity decay time. Typically, an acousto-optic modulator (AOM) is used to switch off the laser beam, although other solutions like

controlled discharging of the voltage on the cavity piezo-electric transducer [153] or fast scanning of the cavity length over time intervals much less than decay time [154] have been demonstrated. In the cw-CRDS setup described by Romanini et al. [149] the amplitude modulation of the mirror-to-mirror distance was chosen to be less than the cavity mode spacing, so that ring-down events could be observed twice per each modulation period. Under the assumption of a fixed laser frequency, slow thermal drift of the cavity length was compensated with a low-bandwidth feedback circuit by adjusting the mean value of the modulation ramp signal. In an alternative approach [72], the laser frequency was slowly modulated with a small amplitude around the stabilized cavity resonance and transmission through the cavity was monitored. This signal was converted into a histogram of transmission signal thorough the cavity versus optical detuning of the laser frequency. Using a low-bandwidth feedback circuit to actuate the laser frequency, the centroid of this histogram was maintained at zero detuning. In this fashion, slow drift in the laser frequency (relative to the local cavity resonance) was eliminated and a single cavity mode could be excited.

The Pound-Drever-Hall (PDH) method for locking a cw laser to a high-finesse optical resonator was developed in the 1980s [47,155]. By tightly locking the laser frequency to a local cavity resonance using the PDH method, one can achieve relatively high peak signal levels, and increased ring-down signal repetition rates which leads to lower detection limits, $\Delta\alpha$, see Eq. (2), through signal averaging. The PDH technique was first applied to CRDS by Paldus et al. [156]. They used a V-shaped, three-mirror ring-down cavity, in which each of two orthogonal polarizations of light had a unique finesse. In 2002 Fox, Oates and Hollberg [157] implemented the PDH technique to a two-mirror optical resonator. In contrast to the dual-polarization method using a V-shaped cavity, PDH-lock of their laser to the cavity had to be periodically interrupted during the ring-down acquisition process. PDH-lock systems with linear cavities were also used by Leeuwen et al. [158] in 2003 and by Martínez et al. [159] in 2006. Typically, values of tens of kHz were obtained for ring-down repetition rates and noise-equivalent absorption coefficients (NEA) values were decreased to $1.43 \times 10^{-11}\,\mathrm{cm^{-1}Hz^{-1/2}}$ [159]. An alternative approach to the PDH locking method is by diode-laser self-locking using optical feedback from the cavity to the laser [160]. The promising capabilities of optical feedback locking were very recently demonstrated in an example of DFB laser narrowing to yield a relative line width of the order of 1 Hz [161]. In cavity enhanced-spectroscopy experiments the probe laser self-locking techniques were implemented by Morville et al. [162] and Romanini et al. [163].

In many line-shape measurements, the comb of cavity resonances is used as a relative frequency axis for recorded spectra. However, thermal drift of the cavity comb modes can degrade the accuracy of measured line-shape parameters (especially for long averaging times) when unstabilized resonators are used. In 2004 Hodges et al. [71] of NIST demonstrated an approach for high spectral fidelity CRDS line-shape measurements, achieving a resolution that exceeded the accuracy of a wavelength meter (typically a few tens of MHz). By actively locking the mirror-to-mirror distance in the ring-down cavity to a reference He-Ne laser, a relative frequency axis with a long-term stability of 1 MHz was obtained. This corresponds to the long-term stability of an optical path length to within about 3 nm, equivalent to 5×10^{-9} of the cavity length. Even better long-term stability can be achieved with an I_2-stabilized He-Ne laser [164]. The accuracy of the FS-CRDS approach quickly found application in several line-shape studies [27,69,165–169]. In this context, a comprehensive discussion comparing FS-CRDS with single and multimode cw-CRDS techniques was carried out in [170]. Moreover, the reader can find a condensed review of FS-CRDS and studies based on this technique in the recent work of Long et al. [171].

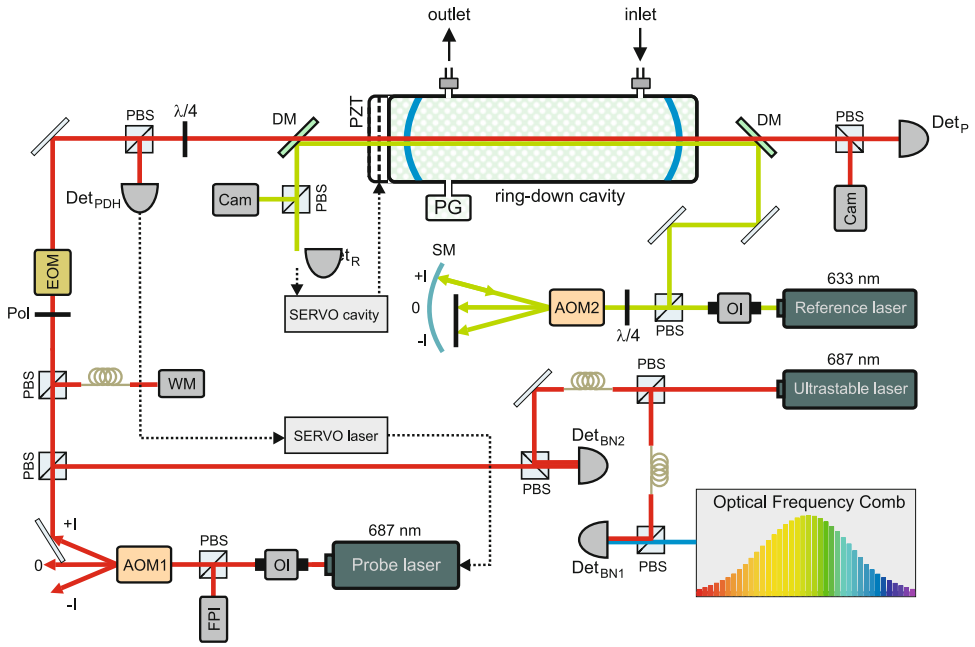

Fig. 2. Scheme of the OFC-assisted PDH-locked FS-CRDS spectrometer: DM – dichroic mirror for separating the probe and the reference beams, AOM1, AOM2 – acousto-optic modulators for the probe beam switching-off and frequency modulation of the reference beam, respectively, EOM – electro-optic modulator for the probe beam phase modulation, FPI – Fabry-Pérot interferometer for controlling a single-mode work of the probe laser, $\mathrm{Det_P}$ – probe beam detector, $\mathrm{Det_R}$ – reference beam detector, $\mathrm{Det_{PDH}}$ – probe beam detector in the PDH method, $\mathrm{Det_{BN1}}$ – comb to ultra-narrow laser beatnote detector, $\mathrm{Det_{BN2}}$ – probe to ultra-narrow laser beatnote detector, Cam – camera to observe transverse modes of the cavity, WM – wavelength meter, PZT – piezo-electric transducer, PG – pressure gauge, OI – optical isolator, PBS – polarizing beam splitter , $\lambda/4$ – quarter-wave plate, Pol – polarizer, SM – spherical mirror.

4 PDH-locked FS-CRDS system

The realization of cavity length stabilization in the FS-CRDS scheme in the way proposed in [71,72] requires double-coated cavity mirrors in order to yield relatively high and low losses for the reference and probe laser, respectively. The feedback error signal used by the cavity length-stabilization servo is obtained by demodulation of the frequency-modulated reference power signal that is transmitted through the cavity. Typically, the cavity resonances at the reference laser wavelength (633 nm) are approximately 3 MHz full-width at half-maximum (FWHM). The frequency modulation (realized using a double-passed AOM) is set to a modulation depth that is several times that of the cavity mode width. In this fashion the FS-CRDS length-stabilization servo [72] enables one to track variations in the reference laser frequency, thus providing step sizes, limited by frequency stability of the HeNe, that are far less than the cavity mode spacing.

The FS-CRDS technique described here was employed four years ago in a high-resolution CRDS developed at the National Laboratory FAMO in Toruń [66–69]. A conception of the current experimental setup is illustrated in Fig. 2. The main part of our spectrometer is a high-finesse ($F = 12600$) optical cavity filled with O_2 gas

with a guaranteed purity of 99.999%. Double-coated, spherical, super-polished mirrors comprising the ring-down cavity, in a non-confocal configuration, are placed 73 cm apart, giving a cavity free spectral range (FSR) of 203 MHz. The mirror coating for the probe laser, an external-cavity diode laser (687 nm), has a reflectivity of $R^{(687)} = 0.99975$, whereas the reflectivity of the reference laser, a polarization stabilized HeNe laser (633 nm), $R^{(633)} = 0.95$. These values correspond to cavity mode FWHMs of 17 kHz and 3.4 MHz, respectively. In order to lock the cavity to the HeNe laser, the HeNe laser frequency is modulated by an AOM operated in first-order diffraction. Angular displacement of the reference beam during modulation is eliminated by application of a double-passed configuration through the AOM. The cavity servo system consists of the PI regulator and the low-pass filter at the input of the cavity piezo-electric transducer, for which the bandwidth is less than 100 Hz. This arrangement allows us to compensate for slow temperature-induced drift of the cavity length and to avoid the transfer of high-frequency noise of the reference laser to the cavity. Ring-down events are recorded by a photodiode with a bandwidth of 10 MHz and are stored in the memory of a fast analog-to-digital converter (ADC). The probe laser beam is switched-off by another AOM having a 50 dB extinction ratio and switching time of 50 ns. The AOM is fast enough so that one can neglect the influence of the beam switch-off time system on the measured light decay. For the 250 ppm-loss mirrors, the typical decay time constant for an empty cavity is about 9.7 μs.

In 2011 we improved the FS-CRDS system by applying a PDH lock of the probe laser to the ring-down cavity. More details about the Pound-Drever-Hall-locked FS-CRDS (PDH-locked FS-CRDS) setup can be found in [67]. To realize the PDH method, we use an electro-optic modulator (EOM) to generate first-order sidebands at 20 MHz. The optical heterodyne signal between the probe laser light reflected from the entrance mirror of the cavity and the light leaking out of the ring-down cavity is detected with a photodiode with a bandwidth of 125 MHz. The optical heterodyne signal is demodulated by mixing with a 20 MHz reference signal, to yield the PDH error signal. Careful adjustment of the phase between the optical heterodyne signal and the reference signal as well as the choice of the sideband gain produced in the EOM are used to optimize the sensitivity of PDH locking.

A noticeable benefit of the high-bandwidth (2 MHz) PDH lock of the probe laser is a substantial increase in intra-cavity power. This is a direct consequence of narrowing the laser linewidth from its free-running value of 300 kHz to approximately 20 kHz. Increasing the coupling efficiency, which was enabled by the PDH lock, leads to a nearly 1000-fold increase in the ring-down repetition rate up to about 14 kHz. To quantify the optimal number of ring-down events over which to average (to minimize the uncertainty in τ), we computed the Allan variance [172] when the laser frequency was stabilized by the PDH method. From the results we estimate a NEA of 7×10^{-11} cm^{-1}Hz$^{-1/2}$ for the PDH-locked FS-CRDS spectrometer [67]. This NEA represents a 15-fold improvement by comparison to the previous FS-CRDS version, for conditions of similar mirror reflectivity, detector and digitizer noise.

The improved measurement precision for the PDH-locked FS-CRDS system enabled us to detect small systematic distortions that were sometimes evident in the initial portion of the ring-down decay signals [69]. This resulted from nonlinearity caused by a malfunctioning ADC which was used to record the ring-down signals. It is worth noting that residual, non-exponential behavior of the ring-down decay signals is an important problem if line-shape parameters are to be measured with uncertainties at the sub-percent level. The presently used ADC board used with the PDH-locked FS-CRDS system allowed us to reduce this statistical error to less than 0.5%. The reader interested in further discussion of these issues should refer to the work [69].

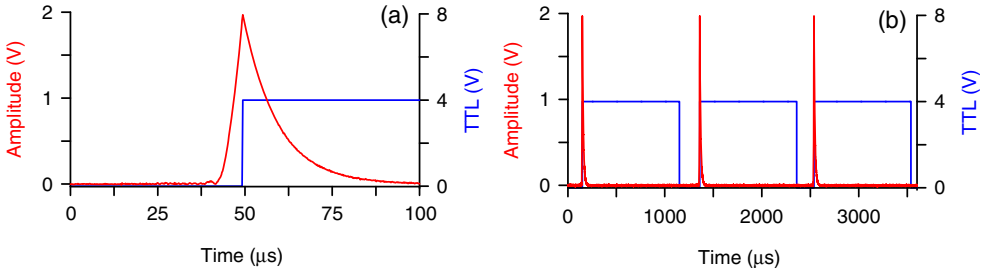

Fig. 3. Stability of ring-down decay signals with periodically interrupted PDH lock. (a) Ring-down decay event characterized by the time constant of 9.7 μs, recorded over the time interval of 55 μs. (b) Demonstration of the longest laser beam switch off time of 1 ms enabled by means of the PDH error signal offset-correction procedure [68] applied to the PDH-locked FS-CRDS system.

Continuous alternation of the probe beam power in CRDS measurements (with a linear optical cavity where only one beam polarization is used) can lead to instability in the PDH servo. This problem was observed by many researchers [157–159] and has been recognized as a major limiting factor for the sensitivity of linear cavities in CRDS systems with the PDH lock. We investigated this instability by inspecting the PDH error signal, and we found that the error signal offset leading to the asymmetry in the locking range was the main source of instability in the servo during its permanent interruption. In Fig. 3(a) we present typical ring-down events for the empty cavity recorded during the 55 μs-long laser beam switching off time. Like others we found that this interval was too long to assure stable operation of the PDH servo. However, after application of our offset correction procedure, described in details in [68], we were able to switch off the laser beam for times longer than 1 ms, as shown in Fig. 3(b). It is worth noting that the ability to measure such long signal decays opens up new possibilities for the development of the PDH-CRDS systems with ultra high reflectivity mirrors, with an emphasis on improved sensitivity.

In CRDS experiments where the spectrometer frequency axis is actively controlled relative to a frequency reference and in which measurement conditions are statistically stationary, long-term averaging of spectra following the white noise statistics is a natural step towards improved precision. Recently we have demonstrated a signal-to-noise ratio (SNR) of 220000 as a result of averaging 1040 spectra [74]. We believe that this is the highest SNR ever reported in optical spectroscopy. In [74] we also presented a detection limit of 2.4×10^{-11} cm^{-1} obtained for the PDH-locked FS-CRDS spectrometer after spectrum averaging. This high sensitivity enables measurement of line intensities lower than 10^{-30} cm^{-1}/(molecule cm^{-2}). In Fig. 4(a) we compare the low-intensity (2.716×10^{-29} cm^{-1}/(molecule cm^{-2})) R41 R41 O_2 B-band line recorded as a single spectrum and after averaging 405 spectra, respectively. To illustrate the tremendous progress achieved in the sensitivity of our spectrometer, we plotted in Fig. 4(b) residuals obtained from SDNGP fits for the R7 Q8 O_2 line. This comparison illustrates a reduction of more than two orders of magnitude in statistical noise. It should be noted that there is still room for improvement in lowering our detection limit. In a recent CRDS experiment, Kassi and Camparague [173] achieved a detection limit of 5×10^{-13} cm^{-1} by averaging 6000 spectral scans acquired over a 4 day time interval and by using ultra-low-loss mirrors with a reflectivity of 0.999993. We note, however, that these experiments were implemented using an unstabilized ring-down cavity, which precludes application to the types of line-shape studies discussed herein.

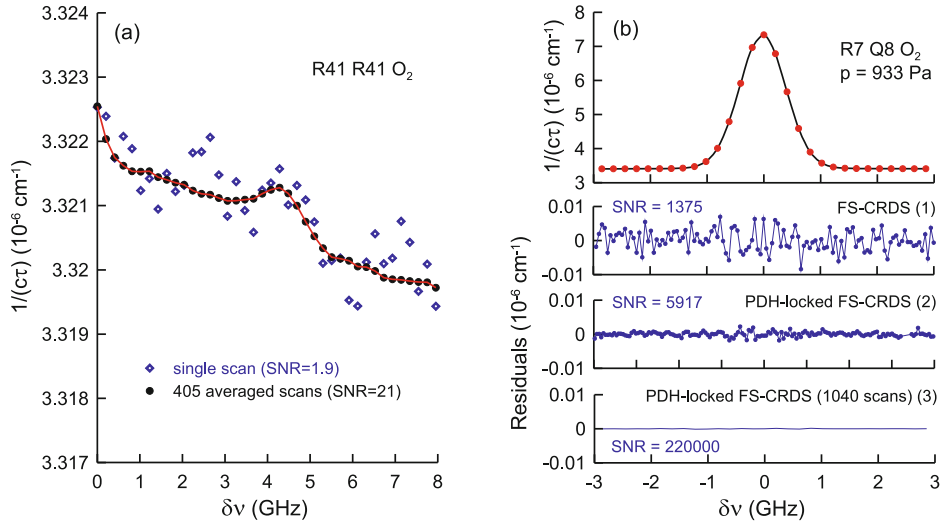

Fig. 4. (a) The single and averaged spectrum for the R41 R41 O_2 B-band line measured at a pressure of 2.67 kPa and fit by the Voigt profile. The interference structure (etalon) seen in the case of single scan was incorporated into line-shape analysis in the case of averaged 405 scans. (b) The spectrum of the R7 Q8 line of the O_2 B-band measured at a pressure of 933 Pa for consecutive versions of our FS-CRDS spectrometer and fit with the SDNGP profile. (1) FS-CRDS from 2010 [66]. (2) PDH-locked FS-CRDS from 2011 [67–69]. (3) PDH-locked FS-CRDS equipped with PDH error signal offset correction system which allowed for long-term averaging of 1040 spectra (from 2012) [74]. The SNR is defined as the ratio of an absorption coefficient in the line peak with the slope and background subtracted to the standard deviation of the random noise.

5 Optical frequency comb-assisted PDH-locked FS-CRDS

The broadband comb of sharp emission lines with precisely known absolute frequencies produced by an OFC can be used as a frequency ruler for cw-laser spectroscopy. Such OFC-assisted techniques have been used for measurements of a variety of atomic [55,174–177] and molecular systems [55,178–180], in the wavelength range from the mid-IR [181] to the extreme ultra-violet [182].

In order to measure absolute frequencies of O_2 B-band transitions, the PDH-locked FS-CRDS spectrometer was linked to an OFC with a rubidium frequency standard (*MenloSystems*[1]*, model: FC1500*). The unknown FS-CRDS probe laser frequency f can be determined by reference to the OFC as follows:

$$f = \pm 2 \times f_0 + n \times f_{\mathrm{rep}} \pm f_{\mathrm{beat}}, \tag{3}$$

where n is the comb tooth number, $f_{\mathrm{rep}} \approx 250\,\mathrm{MHz}$ is the repetition frequency of femtosecond-laser pulses, f_0 is the comb carrier-envelope offset frequency and f_{beat} is the measured heterodyne beat frequency between the n-th comb tooth and probe laser. The factor of two multiplying f_0 corresponds to doubling of the comb spectrum from 1380 nm to the useful measurement range of 690 nm. In our first OFC-assisted experiment, the absolute laser frequency was measured at the beginning and at the

[1] Manufacturers and product names are listed solely for completeness. These specific citations neither constitute an endorsement of the products nor imply that similar products from other companies would be less suitable.

end of each scan of the absorption line [70]. The absolute frequency axis was then calculated from the known mode spacing of the actively stabilized cavity. This approach was simpler than manually tuning f_{rep} or f_0 whenever f_{beat} is ± 5 MHz or more away from 30 MHz center frequency limit set by frequency counter filters. However, this approach had a drawback, because the accuracy of the frequency axis was limited by the long-term stability ± 1.5 MHz of the reference laser to which the ring-down cavity length was stabilized. We found that that small drifts in the reference laser occurred on time scales shorter than 20 min (corresponding to time needed for 8 GHz scans comprising 160 measurement steps (see Fig. 2 in [70])), and consequently its adverse influence on the line-position determination and line-shape fidelity could not be ignored. Therefore, our measured O_2 transition frequencies [70] were limited by the reference laser stability and had combined standard uncertainties in the range of 0.9–2.9 MHz.

We improved the accuracy of line position measurements by an order of magnitude using an ultra-narrow reference laser [183] with a long-term stability of 1 MHz/h (see Fig. 2). In this approach [184], we simultaneously measured two heterodyne beat signals: one between the reference laser and the comb f_{BN1} and another between the reference laser and the probe laser f_{BN2}. With this technique the unknown probe laser frequency is:

$$f = \pm 2 \times f_0 + n \times f_{\mathrm{rep}} \pm f_{\mathrm{BN1}} \pm f_{\mathrm{BN2}}. \tag{4}$$

It is also beneficial to independently and continuously measure the comb-to-reference laser heterodyne beat frequency, because there is no need to readjust the OFC f_{rep} when this frequency is outside the bandwidth of the frequency counter. On the other hand, the slow thermal drift of the ultra-narrow reference laser frequency is taken into account by simultaneous measurement of f_{BN1} and f_{BN2}. This technique allows us to record absorption spectra with an absolute frequency value at each measurement point. In this way, the frequency axis accuracy is limited only by the short-term stability of the reference HeNe laser frequency (± 250 kHz in the time scale of 3 seconds, corresponding to delay between ring-down events and absolute frequency measurements) to which the ring-down cavity is locked. In Ref. [184] we demonstrated line positions with combined uncertainties of 450 kHz, which are the lowest so far obtained for the O_2 B-band. This combined uncertainty was dominated by systematic error of our Rb frequency reference. Determination of the extrapolated to zero pressure line position was done using line profiles measured in several pressures and allowed us to obtain a precision of about 30 kHz. In the meantime a similar experiment was performed at NIST [164], where a combined standard uncertainty of 9 kHz in measured line position was demonstrated.

6 Line-shape measurements

Modern spectroscopy experiments that have a well-characterized frequency axis, a linear detection system and a well-known or negligible instrument function are required for strict tests of line-shape models. For several decades, differential frequency generation (DFG) spectroscopy provided precise experimental data in the near- and mid-infrared regions [185,186], yielding spectrum SNRs as high as 10000 [187]. This level of performance enabled careful tests of speed-dependent effects, correlations between velocity-changing and dephasing collisions, as well as line-mixing [78,79,101–103,188–191,193–200] and collision-time asymmetry [125,188,201–211] in observed line shapes [106,122,212–215]. Similarly, tunable diode lasers allowed for the verification of complex line-shape models in the visible and near-infrared regions [86,123,126,216–218]. The application of FS-CRDS spectroscopy opened new possibilities because of its ultra-high sensitivity and high-fidelity frequency axis. These

investigations are strongly motivated by applications in atmospheric remote sensing, where weak absorption lines are used and where there are increasingly demanding data requirements for line-shape parameters, line intensities and line positions. It is in this context, that the creation of a new generation of atmospheric databases is being discussed. Many sophisticated line-shape models, more advanced than the commonly used the Voigt profile, were tested at laboratory conditions with an ultra-high SNR to provide line parameters of CO_2, H_2O, O_2 and many other atmospheric gas species with low uncertainties [27,69,165,167–169]. Typical standard uncertainties of collisional line broadening coefficients and line intensities achieved in FS-CRDS experiments are in the range of 0.3%–2.2% and 0.3%–0.6%, respectively [69,165,167,170]. Moreover, the newly developed comb-assisted experiments are beginning to provide more accurate data on line positions, which are particularly important for atmospheric research. As noted above, the standard uncertainty of these line position measurements is now of the order of hundreds [70,184] or even several kHz [164,180].

Many groups have reported the limitations of using the Voigt profile in the line-shape analysis [11,13,17,122,123,126,187,214,217,219]. It was shown that even for low gas pressures, deviations from this profile are visible when the experimental precision is sufficiently high [48,220]. The need for careful line-shape analysis also is appreciated by researchers involved in the Doppler-broadening thermometry. Determination of the Boltzmann constant by means of Doppler width measurements [28–31,221] demands rigorous treatment of the line profile. It was found that even for low pressure conditions, generally below 1 Pa, experimental line profiles are far from the expected Gaussian profile. As discussed in [35,36,222] the Voigt profile does not accurately describe measured line shapes. In order to determine the Doppler width with a relative uncertainty better than 10^{-6}, we quantified the importance of the proper choice of line-shape model, the range of gas pressures, as well as the spectral range of the measurements [34].

Although the recently obtained precision of 6.4×10^{-6} [223] is close to the combined uncertainty obtained by Moldover et al. in 1988, in an acoustic gas thermometry experiment [224], there remain important systematic uncertainties (some of which are related to the line-shape) in the spectroscopic measurement of the Boltzmann constant.

The potential of FS-CRDS spectroscopy as a technique for high-precision line-shape investigation was demonstrated in a study of the H_2O line of the 10687.36 cm^{-1} transition perturbed by SF_6 at pressures of 6.7–53.3 kPa [11]. The measured line shapes and fit residuals (for pressure of 26.7 kPa corresponding to SNR of 1000) are shown in Fig. 5(a). The VP and BBP, which are symmetric speed-independent profiles, were not able to fit properly experimental data. This result was caused mostly by speed dependence of the collisional shifting, which was especially strongly manifested in the case of high mass ratio $\beta \sim 8$ and large pressure shifting coefficient of 10 MHz/kPa. The speed-dependent Voigt profile (SDVP) fitted to the data captured the most of the line-shape asymmetry. Application of theoretical models that include both the speed dependence of collisional shifting as well as correlations, in the case of rigid-sphere (CSDBBP) and hard (CSDNGP) collision models led to a nearly perfect fit within the precision of the measurements, but interpretation of obtained line-shape parameters, particularly the Dicke narrowing parameter is different for both of these profiles. More details about the $H_2O + SF_6$ line-shape study can be found in [11].

The ability to extract quantitative information about molecular dynamics from line-shape analysis is obviously limited by the SNR of the measured spectra. For instance we cannot definitively say whether the CSDBBP or the CSDNGP better describes the experimental data on the basis of the last two residuals which are presented in Fig. 5(a). Improvements which were made recently in our spectrometer and which led to its extremely high precision allowed us to investigate these line-shape

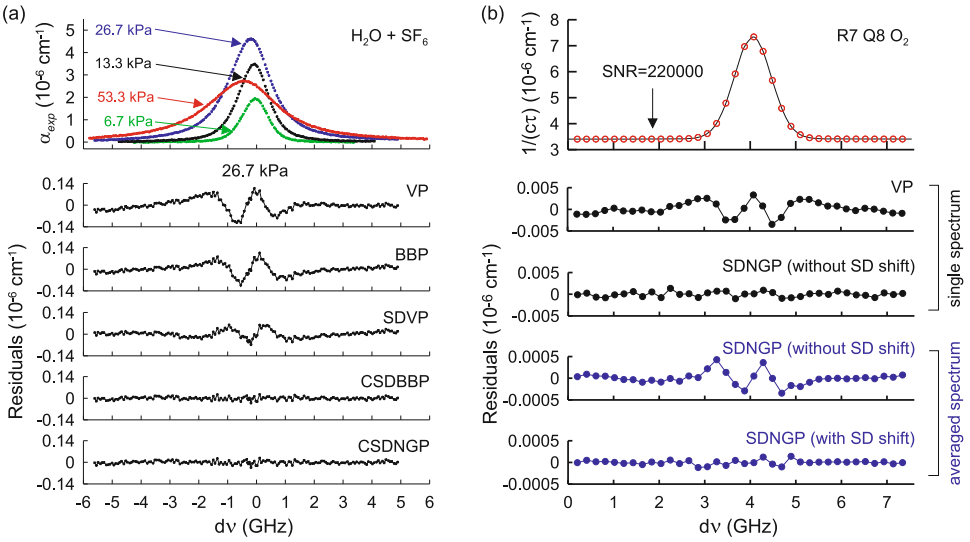

Fig. 5. (a) Experimental profiles of the H_2O 10687.36 cm^{-1} line perturbed by SF_6 at different pressures. Below, residuals from fits of the VP and more complex theoretical line-shape models, obtained at a pressure of 26.7 kPa. (b) The averaged spectrum of the R7 Q8 O_2 B-band line measured at a pressure of 933 Pa and fit with the VP and SDNGP line-shape models. The first two residuals below the spectrum correspond to the single spectrum of the line. The other two residuals were obtained after averaging 1040 scans of the line. For the case of the averaged spectrum, the speed dependence (SD) of the collisional shift was considered in the SDNGP line-shape analysis.

effects more closely. To illustrate this new level of performance, we show in Fig. 5(b) measured spectra for the R7 Q8 O_2. These data yielded a SNR = 220000. The lower panels show the residuals for the VP and SDNGP fits, both for individual and averaged (N= 1040) spectra. The signal-to-noise ratio of 7800 for an individual spectrum is sufficiently high to observe the typical "w" structure on the residuals in case of the VP fit. Moreover, with this precision the SDNGP line-shape function without the speed dependence of collisional shift adequately models molecular collisions, as evidenced by the flat residuals in case of the SDNGP fit. However, the 28-fold improvement of the SNR value offered by averaging the spectra gave fresh insight into analysis of this line. Specifically, the third set of residuals in Fig. 5(b) revealed a subtle line-shape asymmetry. We could remove this asymmetry by incorporating the SDNGP model with the speed dependence of the collisional shift and by incorporating etaloning effects. A more detailed discussion of the underlying analysis is given in [74]. We found that the collisional shift is expected to be more than 20 times smaller than the collisional width of γ_L = 26.546(41) MHz. To our knowledge this is the smallest asymmetry ever observed for a self-broadened line. We assigned this asymmetry to the speed dependence of collisional shift, but as mentioned above other effects which cannot be ignored may also play a role.

In Fig. 6 the dependence of the collisional broadening coefficient γ_L/N on the total angular momentum quantum number J'' is presented. The VP, GP and SDVP line-shape functions were fit to six O_2 measured lines. These results reveal a relatively large difference of about 25% between the VP and more complex GP and SDVP profiles, further indicating limitations of the VP when used in databases such as HITRAN. To overcome the problem of the correlation between line-shape parameters (which is especially evident at small gas pressures), a multispectrum fitting procedure was

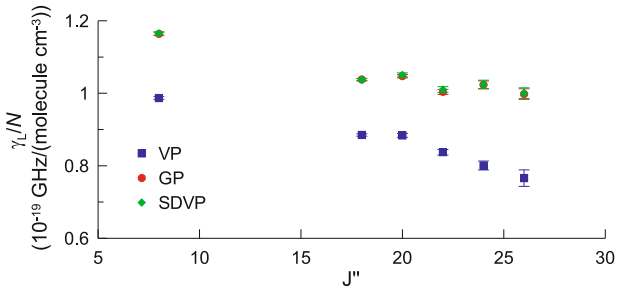

Fig. 6. The dependence of the collisional self-broadening coefficient γ_L/N vs. the angular momentum quantum number J'' for the six chosen O_2 B-band lines and three investigated line-shape models: VP, GP and SDVP. The symbol $''$ refers to the lower energy state.

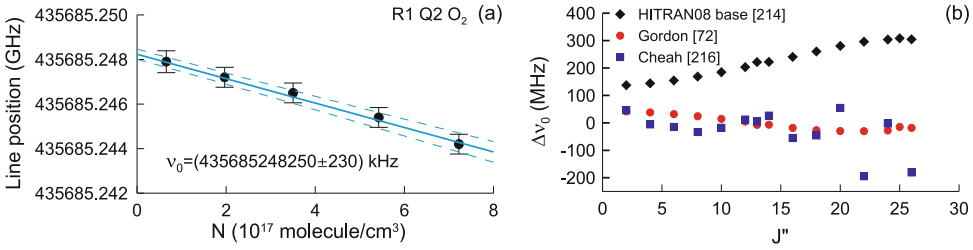

Fig. 7. Absolute line position measurements obtained with the comb-assisted PDH-locked FS-CRDS spectrometer. (a) Dependence of the line position of the R1 Q2 O_2 line on O_2 concentration. Error bars correspond to standard uncertainties, the solid blue line is the weighted linear regression and the dashed blue lines are confidence bounds. ν_0 is the line position extrapolated to zero concentration. (b) Differences between line positions determined in the experiment and values published elsewhere. The symbol J'' is the total angular momentum quantum number for the lower energy state.

employed. The technique was first introduced to the line-shape analysis by Benner [75] using the Voigt profile. In Ref. [9] it was demonstrated that the multi-spectrum fitting is especially useful for the line-shape analysis that apply more advanced profiles like the CSDARSP.

The high precision and accuracy of our spectrometer together with the stable frequency axis and advanced line-shape analysis also enabled us to provide line intensity data with relative standard uncertainties of approximately 0.3%. This level of accuracy meets demanding expectations of the atmospheric remote sensing. Also, we should note that such a low uncertainty in line intensities is not guaranteed by atmospheric databases like HITRAN [225] or GEISA [226].

The results of our O_2 B-band absolute transition frequency measurements obtained with the comb-assisted PDH-locked FS-CRDS spectrometer are presented in Fig. 7. The newest results achieved with the ultra-narrow laser incorporated into the experimental system [184] provided an absolute line position combined uncertainty of about 230 kHz [see graph (a)], which is almost 5 times lower than that obtained in our previous paper [70]. In graph (b) we compare our results to the O_2 B-band line positions data published elsewhere. Our results were most consistent with those of Gordon et al. [73], although we find a systematic difference of about 30 MHz. This value is much greater than the line position uncertainties (0.3–3 MHz). reported in [73]. The data of Cheah et al. [227] are scattered around our values. Moreover, their position for the R25 R25 line differs from ours by about 2 GHz and was not included in the graph. In general, we have found large differences (in the range of 170–300 MHz)

between our measurements and HITRAN [225] line positions. In many cases, however, these differences are consistent with the uncertainties given in HITRAN.

As demonstrated herein, it is clear that optical frequency comb-assisted, PDH-locked FS-CRDS [70,164,184] yields spectroscopic line parameter data with sub-percent relative uncertainties. However, achieving such high accuracy requires that one go beyond a VP-based line-shape analysis, and therefore new spectroscopic databases will need to incorporate more advanced line-shape models. Choosing an appropriate line profile for this purpose involves a tradeoff between physical correctness and simplicity of use. Moreover, the chosen profile should allow users to incorporate the maximum amount of existing high accuracy data.

The SDNGP [126] and CSDNGP [17], which are based on the hard-collision model, are relatively easy to calculate and have been shown to work well in modeling data [11,17,69,126,167,169,213,214,228–233] that have signal-to-noise ratios up to 3000:1, especially when the perturber-to-absorber mass ratio is close to unity. The main justification for using a hard collision model is its simplicity and its consistency with basic statistical rules. However, the hard-collision assumption is an oversimplification and is inconsistent with the physics of intermolecular collisions. Conversely, the GP [82] is often used for data analysis, because the soft collision model has a physical justification for systems with small perturber-to-absorber mass ratio.

It was verified experimentally [7–9,13,129] and by comparison with more realistic molecular dynamics simulations [95,96,111,112], and billiard-ball model calculations [93] that the combination of hard- and soft-collision models like those in the RSP [84,85,127–130,234] and the KSP [87,88,97,99,234,235] can reasonably mimic properties of real collisions over a wide range of conditions. Therefore, we propose that the CSDARSP [129,130] is a sufficiently general profile for the analysis of high-accuracy spectroscopic line parameter data as it was already demonstrated in Refs. [7–9,129]. This profile has several attractive properties. The CSDARSP [129,130] is given by an analytical expression. In one limiting case, it can be simplified to the easily-calculated CSDNGP [17,126], and in another it can be simplified to the SDGP [125] which was already used in several experimental studies [6,12,13,17,121,220,236–240]. The SDGP profile can be further simplified to the GP which is widely used in line-shape studies. Finally, the CSDARSP can be used in a multispectrum data analysis fitting technique [9] and it can describe spectra that span a wide range of physical conditions [7,8,129]. Thus, of the many available theoretical line profiles, we believe that the CSDARSP is the most appropriate choice for incorporation into high-accuracy spectroscopic databases.

7 Future prospects

Over the last decade the FS-CRDS method has proven its applicability to precise and accurate spectral line-shape studies. As was demonstrated here, this approach can yield spectra with extremely high signal-to-noise ratios. However, there remains the problem of quantifying systematic errors in CRDS spectra. Indeed, the fit quality of the theoretical line-shape models to measured spectra is high, with levels of up to 80000 [74] having been demonstrated. However, it should be noted that systematic instrumental errors can confound the real line-shape. The nature of relatively complicated theoretical line-shape models having many fitted parameters can still lead to a high quality of the fit, but the physical meaning of the parameters may be lost if unaccounted-for instrumental distortions remain. Therefore, it is difficult to estimate the total uncertainty of line-shape parameters obtained from fits to high SNR spectra. It was demonstrated in [69] that residual nonlinearity of the ring-down events which are caused by experimental artifacts can be important with regard to distortion of

measured spectra. A thorough investigation of this problem is crucial to reach the limiting case where the measurement accuracy matches the measurement precision.

The PDH-locked FS-CRDS technique can be used for verification of the spectral line-shape theory with a relative precision better than 10^{-5}, especially in the case of very weak molecular transitions. It is especially suitable for characterizing weak molecular lines that are important in atmospheric research, satellite remote sensing of greenhouse gases, and climate change studies. Given the advances in quantitative spectroscopy afforded by techniques such as FS-CRDS, we can now quantify limits of applicability of line-shape models that incorporate Dicke narrowing and speed-dependent collisional broadening and shifting. It is expected that these generalized line-shape models will be used in a growing number of applications. Of fundamental importance will be an ultimate test of *ab initio* line-shape calculations that are based on solution of the transport/relaxation equation [92,135] or molecular dynamic simulations [14,15]. Such experimental validation of fundamental theories will deepen our understanding of physical mechanisms that lead to formation of spectral line shapes.

In recent years, there has been an increasing need for new databases that store spectroscopic data with sub-percent accuracy. To provide such accuracy, high quality spectrometers like described here the PDH-locked FS-CRDS assisted by the optical frequency comb have to be used. A next-generation spectroscopic database needs to have the basic functionality that has made HITRAN so successful, while at the same time it must go beyond use of the Voigt profile. We expect that extension of this and other databases to incorporate more advanced line profiles will enable sub-percent-level uncertainties in calculations of the synthetic spectra. In our opinion, the CSDSRSP is a good candidate for a basic line-shape model that could be incorporated into the next-generation database. There have already been several line-shape studies using the CSDARSP or its limiting cases. Indeed, it has been demonstrated that this profile fits experimental line shapes with a relative precision better then 10^{-3} (relative standard deviation from fit residuals). However, further tests of the CSDARSP on a wide class of molecular systems and its comparison with alternative approaches need to be realized.

Finally, we emphasize that the ultra-precise spectroscopic measurement and line-shape analysis techniques reviewed here are expected to enable the realization of new optical standards. These include a redefinition of the temperature scale related to measured Doppler widths and standards for an amount of substance in terms of measured line intensities.

This work was partially supported by the Foundation for Polish Science TEAM Project cofinanced by the EU European Development Fund and by the National Science Center, Project No. DEC-2011/01/B/ST2/00491. The research is part of the program of the National Laboratory FAMO in Toruń, Poland. A. Cygan is partially supported by the Foundation for Polish Science START Project.

References

1. C.E. Miller, L.R. Brown, R.A. Toth, D. Chris Benner, V. Malathy Devi, C.R. Phys. **6**, 876 (2005)
2. D. Crisp, R.M. Atlas, F.-M. Breon, L.R. Brown, J.P. Burrows, P. Ciais, B.J. Connor, S.C. Doney, I.Y. Fung, D.J. Jacob, C.E. Miller, D. O'Brien, S. Pawson, J.T. Randerson, P. Rayner, R.J. Salawitch, S.P. Sander, B. Sen, G.L. Stephens, P.P. Tans, G.C. Toon, P.O. Wennberg, S.C. Wofsy, Y.L. Yung, Z. Kuang, B. Chudasama, G. Sprague, B. Weiss, R. Pollock, D. Kenyon, S. Schroll, Adv. Space Res. **34**, 700 (2004)
3. M.J. Thorpe, J. Ye, Appl. Phys. B **91**, 397 (2008)

4. M.J. Thorpe, D. Balslev-Clausen, M.S. Kirchner, J. Ye, Opt. Express **16**, 2387 (2008)
5. International Technology Roadmap for Semiconductors, `http://www.itrs.net`
6. P. Duggan, P.M. Sinclair, R. Berman, A.D. May, J.R. Drummond, J. Mol. Spectrosc. **186**, 90 (1997)
7. F. Chaussard, X. Michaut, R. Saint-Loup, H. Berger, P. Joubert, B. Lance, J. Bonamy, D. Robert, J. Chem. Phys. **112**, 158 (2000)
8. F. Chaussard, R. Saint-Loup, H. Berger, P. Joubert, X. Bruet, J. Bonamy, D. Robert, J. Chem. Phys. **113**, 4951 (2000)
9. A.S. Pine, R. Ciuryło, J. Mol. Spectrosc. **208**, 180 (2001)
10. J.-F. D'Eu, B. Lemoine, F. Rohart, J. Mol. Spectrosc. **212**, 96 (2002)
11. D. Lisak, J.T. Hodges, R. Ciuryło, Phys. Rev. A **73**, 012507 (2006)
12. M.D. De Vizia, A. Castrillo, E. Fasci, L. Moretti, F. Rohart, L. Gianfrani, Phys. Rev. A **85**, 062512 (2012)
13. H. Tran, N.H. Ngo, J.-M. Hartmann, R.R. Gamache, D. Mondelain, S. Kassi, A. Camparague, L. Gianfrani, A. Castrillo, E. Fasci, F. Rohart, J. Chem. Phys. **138**, 034302 (2013)
14. J.-M. Hartmann, H. Tran, N.H. Ngo, X. Landsheere, P. Chelin, Y. Lu, A.-W. Liu, S.-M. Hu, L. Gianfrani, G. Casa, A. Castrillo, M. Lepère, Q. Delière, M. Dhyne, L. Fissiaux, Phys. Rev. A **87**, 013403 (2013)
15. J.-M. Hartmann, V. Sirroneau, C. Boulet, T. Svensson, J.T. Hodges, C.T. Xu, Phys. Rev. A **87**, 032510 (2013)
16. S. Green, J. Hutson, J. Chem. Phys. **100**, 891 (1994)
17. A.S. Pine, J. Quant. Spectrosc. Radiat. Transf. **62**, 397 (1999)
18. J.-M. Hartmann, C. Boulet, J. Chem. Phys. **113**, 9000 (2000)
19. C. Luo, R. Wehr, J.R. Drummond, A.D. May, F. Thibault, J. Boissoles, J.M. Launay, C. Boulet, J.-P. Bouanich, J.-M. Hartmann, J. Chem. Phys. **115**, 2198 (2001)
20. R. Wehr, A. Victu, F. Thibault, J.R. Drummond, A.D. May, J. Mol. Spectrosc. **235**, 69 (2006)
21. S. Yu, C.E. Miller, B.J. Drouin, H.S.P. Müller, J. Chem. Phys. **137**, 024304 (2012)
22. S. Kassi, A. Campargue, K. Pachucki, J. Komasa, J. Chem. Phys. **136**, 184309 (2012)
23. E. Kerstel, L. Gianfrani, Appl. Phys. B **92**, 439 (2008)
24. R. Wehr, S. Kassi, D. Romanini, L. Gianfrani, Appl. Phys. B **92**, 459 (2008)
25. A. Castrillo, H. Dinesan, G. Casa, G. Galzerano, P. Laporta, L. Gianfrani, Phys. Rev. A **86**, 052515 (2012)
26. J. Hodgkinson, R.P. Tatam, Meas. Sci. Technol. **24**, 012004 (2013)
27. D.A. Long, D.K. Havey, M. Okumura, C.E. Miller, J.T. Hodges, Phys. Rev. A. **81**, 064502 (2010)
28. C. Daussy, M. Guinet, A. Amy-Klein, K. Djerroud, Y. Hermier, S. Briaudeau, Ch.J. Bordé, C. Chardonnet, Phys. Rev. Lett. **98**, 250801 (2007)
29. G. Casa, A. Castrillo, G. Galzerano, R. Wehr, A. Merlone, D. Di Serafino, P. Laporta, L. Gianfrani, Phys. Rev. Lett. **100**, 200801 (2008)
30. K.M.T. Yamada, A. Onae, F.-L. Hong, H. Inaba, T. Shimizu, C.R. Phys. **10**, 907 (2009)
31. C. Lemarchand, K. Djerroud, B. Darquié, O. Lopez, A. Amy-Klein, C. Chardonnet, Ch. J. Bordé, S. Briaudeau, C. Daussy, Int. J. Thermophys **31**, 1347 (2010)
32. Y.R. Sun, H. Pan, C.-F. Cheng, A.-W. Liu, J.-T. Zhang, S.-M. Hu, Opt. Exp. **19**, 19993 (2011)
33. C.J. Bordé, C. R. Physique **10**, 866 (2009)
34. A. Cygan, D. Lisak, R.S. Trawiński, R. Ciuryło, Phys. Rev. A **82**, 032515 (2010)
35. M.D. De Vizia, L. Moretti, A. Castrillo, E. Fasci, L. Gianfrani, Mol. Phys. **109**, 2291 (2011)
36. M. Triki, C. Lemarchand, B. Darquié, P.L.T. Sow, V. Roncin, C. Chardonnet, C. Daussy, phys. Rev. A **85**, 062510 (2012)
37. W.C. Swann, S.L. Gilbert, J. Opt. Soc. Am. B **19**, 2461 (2002)
38. D.J. Robichaud, J.T. Hodges, P. Masłowski, L.Y. Yeung, M. Okumura, C.E. Miller, L.R. Brown, J. Mol. Spectrosc. **251**, 27 (2008)

39. G. Galzerano, E. Fasci, A. Castrillo, N. Coluccelli, L. Gianfrani, P. Laporta, Opt. Lett. **34**, 3107 (2009)
40. A.A. Madej, P. Dubé, Z. Zhou, J.E. Bernard, M. Gertsvolf, Phys. Rev. Lett. **109**, 203002 (2012)
41. F.J.M. Harren, F.G.C. Bijnen, J. Reuss, L.A.C.J. Voesenek, C.W.P.M. Blom, Appl. Phys. B **50**, 137 (1990)
42. B.A. Paldus, T.G. Spence, R.N. Zare, J. Oomens, F.J.M. Harren, D.H. Parker, C. Gmachl, F. Cappasso, D.L. Sivco, J.N. Baillargeon, A.L. Hutchinson, A.Y. Cho, Opt. Lett. **24**, 178 (1999)
43. A.A. Kosterev, Y.A. Bakhirkin, F.K. Tittel, Appl. Phys. B **80**, 133 (2005)
44. R.N. Zare, Annu. Rev. Anal. Chem. **5**, 1 (2012)
45. J. Ye, L.-S. Ma, J.L. Hall, J. Opt. Soc. Am. B **15**, 6 (1998)
46. T.G. Spence, C.C. Harb, B.A. Paldus, R.N. Zare, B. Willke, R. L. Byer, Rev. Sci. Instrum. **71**, 347 (2000)
47. R.W.P. Drever, J.L. Hall, F.V. Kowalski, J. Hough, G.M. Ford, A. J. Munley, H. Ward, Appl. Phys. B **31**, 97 (1983)
48. D.A. Long, M. Okumura, C.E. Miller, J.T. Hodges, Appl. Phys. B **105**, 471 (2011)
49. E. Gerecht, K.O. Douglass, D.F. Plusquellic, Opt. Express **19**, 8973 (2011)
50. G.G. Brown, B.C. Dian, K.O. Douglass, S.M. Geyer, S.T. Shipman, B.H. Pate, Rev. Sci. Instrum. **79**, 053103 (2008)
51. T. Kessler, C. Hagemann, C. Grebing, T. Legero, U. Sterr, F. Riehle, M.J. Martin, L. Chen, J. Ye, Nature Photonics **6**, 687 (2012)
52. J.-P. Uzan, Rev. Mod. Phys. **75**, 403 (2003)
53. S.G. Karshenboim, Can. J. Phys. **83**, 767 (2005)
54. W. Ubach, R. Buning, K.S.E. Eikema, E. Reinhold, J. Mol. Spectrosc. **241**, 155 (2007)
55. S.A. Diddams, D.J. Jones, J. Ye, S.T. Cundiff, J.L. Hall, J.K. Ranka, R.S. Windeler, R. Holzwarth, T. Udem, T.W. Hänsch, Phys. Rev. Lett. **22**, 5102 (2000)
56. R. Holzwarth, Th. Udem, T.W. Hänsch, J.C. Knight, W.J. Wadsworth, P. St. J. Russell, Phys. Rev. Lett. **85**, 2264 (2000)
57. S.A. Diddams, J. Opt. Soc. Am. B **27**, B51 (2010)
58. N.R. Newbury, Nature Photonics **5**, 186 (2011)
59. T. Gherman, D. Romanini, Opt. Express **10**, 1033 (2002)
60. M.J. Thorpe, K.D. Moll, R.J. Jones, B. Safdi, J. Ye, Science **311**, 1595 (2006)
61. F. Adler, M.J. Thorpe, K.C. Cossel, J. Ye, Annu. Rev. Anal. Chem. **3**, 175 (2010)
62. B. Bernhardt, A. Ozawa, P. Jacquet, M. Jacquey, Y. Kobayashi, T. Udem, R. Holzwarth, G. Guelachvili, T.W. Hänsch, N. Picqué, Nature Photonics **4**, 55 (2010)
63. A. Foltynowicz, P. Masłowski, T. Ban, F. Adler, K.C. Cossel, T.C. Briles, J. Ye, Farraday Discuss. **150**, 23 (2011)
64. A. Foltynowicz, T. Ban, P. Masłowski, F. Adler, Jun Ye, Phys. Rev. Lett. **107**, 233002 (2011)
65. R. Grilli, G. Méjean, C. Abd Alrahman, I. Ventrillard, S. Kassi, D. Romanini, Phys. Rev. A **85**, 051804 (2012)
66. D. Lisak, P. Masłowski, A. Cygan, K. Bielska, S. Wójtewicz, M. Piwiński, J.T. Hodges, R.S. Trawiński, R. Ciuryło, Phys. Rev. A **81**, 042504 (2010)
67. A. Cygan, D. Lisak, P. Masłowski, K. Bielska, S. Wójtewicz, J. Domysławska, R.S. Trawiński, R. Ciuryło, H. Abe, J.T. Hodges Rev. Sci. Instrum. **82**, 063107 (2011)
68. A. Cygan, D. Lisak, S. Wójtewicz, J. Domysławska, R.S. Trawiński, R. Ciuryło, Meas. Sci. Technol. **22**, 115303 (2011)
69. S. Wójtewicz, D. Lisak, A. Cygan, J. Domysławska, R.S. Trawiński, R. Ciuryło, Phys. Rev. A **84**, 032511 (2011)
70. J. Domysławska, S. Wójtewicz, D. Lisak, A. Cygan, F. Ozimek, K. Stec, C. Radzewicz, R.S. Trawiński, R. Ciuryło, J. Chem. Phys. **136**, 024201 (2012)
71. J.T. Hodges, H.P. Layer, W.M. Miller, G.E. Scace, Rev. Sci. Instr. **75**, 849 (2004)
72. J.T. Hodges, R. Ciuryło, Rev. Sci. Instrum. **76**, 023112 (2005)
73. I.E. Gordon, L.S. Rothman, G.C. Toon, JQSRT **112**, 2310 (2011)

74. A. Cygan, D. Lisak, S. Wójtewicz, J. Domysławska, J.T. Hodges, R.S. Trawiński, R. Ciuryło, Phys. Rev. A **85**, 022508 (2012)
75. D. Chris Benner, C.P. Rinsland, V. Malathy Devi, M.A.H. Smith, D. Atkins, JQSRT **53**, 705 (1995)
76. J.-M. Hartmann, C. Boulet, D. Robert, *Collisional Effects on Molecular Spectra: Laboratory Experiments and Model, Consequences for Applications* (Elsevier, Amsterdam, 2008)
77. J. Buldyreva, N. Lavrentieva, V. Starikov, *Collisional Line Broadening and Shifting of Atmospheric Gases: A practical guide for line shape modelling by current semi-classical aproaches* (Imperial College Press, London, 2011)
78. M. Baranger, Phys. Rev. **111**, 481 (1958)
79. M. Baranger, Phys. Rev. **112**, 855 (1958)
80. R.H. Dicke, Phys. Rev. **89**, 472 (1953)
81. J.P. Wittke, R.H. Dicke, Phys. Rev. **103**, 620 (1956)
82. L. Galatry, Phys. Rev. **122**, 1218 (1961)
83. M. Nelkin, A. Ghatak, Phys. Rev. **135**, A4 (1964)
84. S.G. Rautian, I.I. Sobelman, Usp. Fiz. Nauk **90**, 209 (1966)
85. S.G. Rautian, I.I. Sobelman, Sov. Phys. Usp. **9**, 701 (1967)
86. P.L. Varghese, R.K. Hanson, Appl. Opt. **23**, 2376 (1984)
87. J. Keilson, J.E. Storer, Quart. J. Appl. Math. **10**, 243 (1952)
88. D.A. Shapiro, J. Phys. B: At. Mol. Opt. Phys. **33**, L43 (2000)
89. T. Privalov, A. Shalagin, Phys. Rev. A **59**, 4331 (1999)
90. R. Blackmore, J. Chem. Phys. **87**, 791 (1987)
91. D.A. Shapiro, R. Ciuryło, J.R. Drummond, A.D. May, Phys. Rev. A **65**, 012501 (2002)
92. A.D. May, W.-K. Liu, F.R.W. McCourt, R. Ciuryło, J. Sanchez-Fortún Stoker, D. Shapiro, R. Wehr, Can. J. Phys. (2013), doi: 10.1139/cjp-2012-0345
93. R. Ciuryło, D.A. Shapiro, J.R. Drummond, A.D. May, Phys. Rev. A **65**, 012502 (2002)
94. M.J. Lindenfeld, J. Chem. Phys. **73**, 5817 (1980)
95. P.N.M. Hoang, P. Joubert, D. Robert, Phys. Rev. A **65**, 012507 (2002)
96. P. Joubert, P.N.M. Hoang, L. Bonamy, D. Robert, Phys. Rev. A **66**, 042508 (2002)
97. D. Robert, L. Bonamy, Eur. Phys. J. D **2**, 245 (1998)
98. D. Robert, P. Joubert, B. Lance, J. Mol. Struct. **517-518**, 393 (2000)
99. L. Bonamy, H. Tran Thi Ngoc, P. Joubert, D. Robert, Eur. Phys. J. D **31**, 459 (2004)
100. S. Chandrasekhar, Rev. Mod. Phys. **15**, 1 (1943)
101. V.P. Kochanov, JQSRT **66**, 313 (2000)
102. E.W. Smith, J. Cooper, W.R. Chappell, T. Dillon, JQSRT **11**, 1547 (1971)
103. E.W. Smith, J. Cooper, W.R. Chappell, T. Dillon, JQSRT **11**, 1567 (1971)
104. G. Nienhuis, JQSRT **20**, 275 (1978)
105. P.R. Berman, T.W. Mossberg, S.R. Hartmann, Phys. Rev. A **25**, 2550 (1982)
106. A.S. Pine, J. Chem. Phys. **101**, 3444 (1994)
107. P. Joubert, J. Bonamy, D. Robert, J.-L. Domenech, D. Bermejo, JQSRT **61**, 519 (1999)
108. J.P. Looney, R.M. Herman, JQSRT **37**, 547 (1987)
109. R.M. Herman, AIP Conf. Proc. **559**, 237 (2001)
110. L. Demeio, S. Green, L. Monchick, J. Chem. Phys. **102**, 9160 (1995)
111. N.H. Ngo, H. Tran, R.R. Gamache, J. Chem. Phys. **136**, 154310 (2012)
112. N.H. Ngo, H. Tran, R.R. Gamache, J. Chem. Phys. **136**, 189901 (2012)
113. P.R. Berman, J. Quant. Spectrosc. Radiat. Transf. **12**, 1331 (1972)
114. J. Ward, J. Cooper, E.W. Smith, J. Quant. Spectrosc. Radiat. Transf. **14**, 555 (1974)
115. H.M. Pickett, J. Chem. Phys. **73**, 6090 (1980)
116. R.L. Farrow, L.A. Rahn, G.O. Sitz, J.J. Rosasco, Phys. Rev. Lett. **63**, 746 (1989)
117. I. Shannon, M. Harris, D.R. McHugh, E.L. Lewis, J. Phys. B **19**, 1409 (1986)
118. K.J. Ritter, T.D. Wilkerson, J. Mol. Spec. **121**, 1 (1987)
119. F. Rohart, G. Wlodarczak, J.-M. Colmont, G. Cazzoli, L. Dore, C. Puzzarini, J. Mol. Spectrosc. **251**, 282 (2008)

120. P. Duggan, P.M. Sinclair, R. Berman, A.D. May, J.R. Drummond, J. Mol. Spectrosc. **186**, 90 (1997)
121. D. Priem, F. Rohart, J.-M. Colmont, G. Wlodarczak, J.-P. Bouanich, J. Mol. Struct. **517**, 435 (2000)
122. P. Duggan, P.M. Sinclair, A.D. May, J. R. Drummond, Phys. Rev. A **51**, 218 (1995)
123. A. Henry, D. Hurtmans, M. Margottin-Maclou, A. Valentin, J. Quant. Spectrosc. Radiat. Transfer **56**, 647 (1996)
124. R. Ciuryło, R. Jaworski, J. Jurkowski, A.S. Pine, J. Szudy, Phys. Rev. A **63**, 032507 (2001)
125. R. Ciuryło, J. Szudy, R.S. Trawiński, JQSRT **57**, 551 (1997)
126. B. Lance, G. Blanquet, J. Walrand, J.-P. Bouanich, J. Mol. Spectrosc. **185**, 262 (1997)
127. R. Ciuryło, Phys. Rev. A **58**, 1029 (1998)
128. B. Lance, D. Robert, J. Chem. Phys. **109**, 8283 (1998)
129. R. Ciuryło, A.S. Pine, J. Szudy, J. Quant. Spectrosc. Radiat. Transf. **68**, 257 (2001)
130. B. Lance, D. Robert, J. Chem. Phys. **111**, 789 (1999)
131. P. Wcisło, R. Ciuryło, JQSRT **120**, 36 (2013)
132. P. Wcisło, A. Cygan, D. Lisak, R. Ciuryło, Phys. Rev. A (submitted) (2013)
133. R. Ciuryło, A. Bielski, J.R. Drummond, D. Lisak, A.D. May, A.S. Pine, D.A. Shapiro, J. Szudy, R.S. Trawiński, in Spectral Line Shapes, edited by C.A. Back AIP, Melville, NY (2002), p. 151
134. R. Wehr, A. Vitcu, R. Ciuryło, F. Thibault, J.R. Drummond, A.D. May, Phys. Rev. A **66**, 062502 (2002)
135. R. Blackmore, S. Green, L. Monchick, J. Chem. Phys. **91**, 3846 (1989)
136. G. Berden, R. Peeters, G. Meijer, Int. Rev. Phys. Chem. **19**, 565 (2000)
137. B.A. Paldus, A.A. Kachanov, Can. J. Phys. **83**, 975 (2005)
138. G. Berden, R. Engeln, *Cavity Ring-Down Spectroscopy: Techniques and Applications* (Wiley-Blackwell, The Netherlands, 2009)
139. D.A. Jackson, Proc. R. Soc. Lond. A **263**, 289 (1961)
140. A. Kastler, Appl. Opt. **1**, 17 (1962)
141. A. Kastler, Nouv. Rev. d'Optique **5**, 133 (1974)
142. J.M. Herbelin, J.A. McKay, M.A. Kwok, R.H. Ueunten, D.S. Urevig, D.J. Spencer, D.J. Benard, Appl. Opt. **19**, 144 (1980)
143. D.Z. Anderson, J.C. Frisch, C.S. Masser, Appl. Opt. **23**, 1238 (1984)
144. R. Curran, T. Crook, J. Zook, Mater. Res. Soc. Symp. Proc. **105**, 175 (1988)
145. A. O'Keefe, D.A.G. Deacon, Rev. Sci. Instrum. **59**, 2544 (1988)
146. J.T. Hodges, J.P. Looney, R.D. van Zee, Appl. Opt. **35**, 4112 (1996)
147. J.T. Hodges, J.P. Looney, R.D. van Zee, J. Chem. Phys. **105**, 10278 (1996)
148. R.D. van Zee, J.T. Hodges, J.P. Looney, Appl. Opt. **38**, 3951 (1999)
149. D. Romanini, A.A. Kachanov, N. Sadeghi, F. Stoeckel, Chem. Phys. Lett. **264**, 316 (1997)
150. K.K. Lehmann, U.S. Patent No. 5 528 040 (1996)
151. D. Romanini, J. Gambogi, K.K. Lehmann, in 50th International Symposium on Molecular Spectroscopy, edited by T.A. Miller (ACS, Ohio State University, Columbus, OH, 1995), p. 284
152. R.M. Curran, T.M. Crook, D.J. Zook, MRS proceedings **105**, 175 (1987)
153. J.W. Hahn, Y.S. Yoo, J.Y. Lee, J.W. Kim, H.-W. Lee, Appl. Opt. **38**, 1859 (1999)
154. Y. He, B.J. Orr, Chem. Phys. Lett. **319**, 131 (2000)
155. E.D. Black, Am. J. Phys. **69**, 79 (2001)
156. B.A. Paldus, C.C. Harb, T.G. Spence, B. Wilke, J. Xie, J.S. Harris, R.N. Zare, J. Appl. Phys. **83**, 3991 (1998)
157. R.W. Fox, C.W. Oates, L.W. Hollberg, *Stabilizing diode lasers to high-finesse cavities* in *Cavity-Enhanced Spectroscopies*, edited by R.D. Van Zee, J.P. Looney (Academic Press, New York, 2002)
158. N.J. van Leeuwen, J.C. Diettrich, A.C. Wilson, Appl. Opt. **42**, 3670 (2003)

159. R.Z. Martínez, M. Metsälä, O. Vaittinen, T. Lantta, L. Halonen, J. Opt. Soc. Am. B **23**, 727 (2006)
160. P. Laurent, A. Clairon, C. Breant, IEEE J. Quant. Electron. **25**, 1131 (1989)
161. Y. Zhao, Q. Wang, F. Meng, Y. Lin, S. Wang, Y. Li, B. Lin, S. Cao, J. Cao, Z. Fang, T. Li, E. Zang, Opt. Lett. **37**, 4729 (2012)
162. J. Morville, S. Kassi, M. Chenevier, D. Romanini, Appl. Phys. B **80**, 1027 (2005)
163. D. Romanini, M. Chenevier, S. Kassi, M. Schmidt, C. Valant, M. Ramonet, J. Lopez, H.-J. Jost, Appl. Phys. B **83**, 659 (2006)
164. G.-W. Truong, D. Long, A. Cygan, D. Lisak, R.D. van Zee, J.T. Hodges, J. Chem. Phys. **138**, 094201 (2013)
165. J.T. Hodges, D. Lisak, N. Lavrentieva, A. Bykov, L. Sinitsa, J. Tennyson, R.J. Barber, R.N. Tolchenov, J. Mol. Spectrosc. **249**, 86 (2008)
166. D. Lisak, J.T. Hodges, J. Mol. Spectrosc. **249**, 6 (2008)
167. D. Lisak, D.K. Havey, J.T. Hodges, Phys. Rev. A **79**, 052507 (2009)
168. D.A. Long, D.K. Havey, M. Okumura, H.M. Pickett, C.E. Miller, J.T. Hodges, Phys. Rev. A **80**, 042513 (2009)
169. D.A. Long, K. Bielska, D. Lisak, D.K. Havey, M. Okumura, C.E. Miller, J.T. Hodges, J. Chem. Phys. **135**, 064308 (2011)
170. J.T. Hodges, D. Lisak, Appl. Phys. B **85**, 375 (2006)
171. D.A. Long, A. Cygan, R.D. van Zee, M. Okumura, C.E. Miller, D. Lisak, J.T. Hodges, Chem. Phys. Lett. **536**, 1 (2012)
172. D.W. Allan, Proc. IEEE **54**, 221 (1996)
173. S. Kassi, A. Campargue, J. Chem. Phys. **137**, 234201 (2012)
174. T. Udem, J. Reichert, R. Holzwarth, T.W. Hänsch, Phys. Rev. Lett. **82**, 3568 (1999)
175. V. Gerginov, C.E. Tanner, S. Diddams, A. Bartels, L. Hollberg, Phys. Rev. A **70**, 042505 (2004)
176. T.W. Hänsch, J. Alnis, P. Fendel, M. Fischer, C. Gohle, M. Herrmann, R. Holzwarth, N. Kolachevsky, T. Udem, M. Zimmermann, Phil. Trans. R. Soc. A **363**, 2155 (2005)
177. S. Falke, E. Tiemann, C. Lisdat, H. Schnatz, G. Grosche, Phys. Rev. A **74**, 149 (2006)
178. P. Balling, M. Fischer, P. Kubina, R. Holzwarth, Opt. Express **13**, 9196 (2005)
179. S. Bartalini, P. Cancio, G. Giusfredi, D. Mazzotti, P. De Natale, S. Borri, I. Galli, T. Leveque, L. Gianfrani, Opt. Lett. **72**, 988 (2007)
180. G. Galzerano, A. Gambetta, E. Fasci, A. Castrillo, M. Marangoni, P. Laporta, L. Gianfrani, Appl. Phys. B **102**, 725 (2011)
181. P. Cancio, S. Bartalini, S. Borri, I. Galli, G. Gagliardi, G. Giusfredi, P. Maddaloni, P. Malara, D. Mazzotti, P. De Natale, Appl. Phys. B **102**, 255 (2011)
182. A. Cingöz, D.C. Yost, T.K. Allison, A. Ruehl, M.E. Fermann, I. Hartl, J. Ye, Nature **482**, 68 (2012)
183. D. Lisak, A. Cygan, K. Bielska, M. Piwiński, F. Ozimek, T. Ido, R.S. Trawiński, R. Ciuryło, Acta Phys. Pol. A **121**, 614 (2012)
184. J. Domysławska, S. Wójtewicz, A. Cygan, K. Bielska, D. Lisak, P. Masłowski, R.S. Trawiński, R. Ciuryło, Phys. Rev. A (in preparation) (2013)
185. A.S. Pine, J. Opt. Soc. Am. **64**, 1683 (1974)
186. A.S. Pine, J. Opt. Soc. Am. **66**, 97 (1976)
187. R. Wehr, J.R. Drummond, A. D. May, Appl. Opt. **46**, 978 (2007)
188. R. Ciuryło, J. Szudy, Phys. Rev. A **63**, 042714 (2001)
189. A.C. Kolb, H. Griem, Phys. Rev. **111**, 514 (1958)
190. U. Fano, Phys. Rev. **131**, 259 (1963)
191. A. Ben-Reuven, Phys. Rev. **141**, 34 (1966)
192. A. Ben-Reuven, Phys. Rev. **145**, 7 (1966)
193. A. Ben-Reuven, Adv. Chem. Phys. **33**, 235 (1975)
194. R.G. Gordon, J. Chem. Phys. **46**, 448 (1967)
195. R.G. Gordon, R.P. McGiunis, J. Chem. Phys. **49**, 2455 (1968)
196. E.W. Smith, J. Chem. Phys. **74**, 6658 (1981)
197. P.W. Rosenkranz, IEEE Trans. Antennas Propag. **23**, 498 (1975)

198. A.S. Pine, JQSRT **57**, 145 (1997)
199. R. Ciuryło, A.S. Pine, JQSRT **67**, 375 (2000)
200. W.F. Wang, J.M. Sirota, J. Chem. Phys. **116**, 532 (2002)
201. P.W. Anderson, J.D. Talman, Bell Telephone Syst. Techn. Publ. **3117**, 1955 (unpublished)
202. J. Szudy, W.E. Baylis, JQSRT **15**, 641 (1975)
203. J. Szudy, W.E. Baylis, JQSRT **17**, 681 (1977)
204. J. Szudy, W.E. Baylis, Phys. Rep. **266**, 127 (1996)
205. A. Royer, Acta Phys. Pol. A **54**, 805 (1978)
206. B.N.I. Al-Saqabi, G. Peach, J. Phys. B **20**, 1175 (1987)
207. P. Marteau, C. Boulet, D. Robert, J. Chem. Phys. **80**, 3632 (1984)
208. A. Royer, Acta Phys. Pol. A **54**, 805 (1978)
209. P.S. Julienne, F.H. Mies, Phys. Rev. A **34**, 3792 (1986)
210. C. Boulet, P.-M. Flaud, J.-M. Hartmanna, J. Chem. Phys. **120**, 11053 (2004)
211. R.S. Trawiński, R. Ciuryło, J. Szudy, Phys. Rev. A **74**, 022716 (2006)
212. S. Nazemi, A. Javan, A.S. Pine, J. Chem. Phys. **78**, 4797 (1983)
213. A.S. Pine, V.N. Markov, J. Mol. Spectrosc. **228**, 121 (2004)
214. D. Lisak, G. Rusciano, A. Sasso, Phys. Rev. A **72**, 012503 (2005)
215. H. Tran, D. Bermejo, J.-L. Domenech, P. Joubert, R.R. Gamache, J.-M. Hartmann, J. Quant. Spectrosc. Radiat. Transfer **108**, 126 (2007)
216. R.S. Eng, A.R. Calawa, T.C. Harman, P.L. Kelley, A. Javan, Appl. Phys. Lett. **21**, 303 (1972)
217. F. Thibault, A.W. Mantz, C. Claveau, A. Henry, A. Valentin, D. Hurtmans, J. Molec. Spectrosc. **246**, 118 (2007)
218. D. Hurtmans, A. Henry, A. Valentin, C. Boulet, J. Molec. Spectrosc. **254**, 126 (2009)
219. G. Casa, R. Wehr, A. Castrillo, E. Fasci, L. Gianfrani, J. Chem. Phys. **130**, 184306 (2009)
220. M.D. De Vizia, F. Rohart, A. Castrillo, E. Fasci, L. Moretti, L. Gianfrani, Phys. Rev. A **83**, 052506 (2011)
221. A. Merlone, F. Moro, A. Castrillo, L. Gianfrani, Int. J. Thermophys. **31**, 1360 (2010)
222. A. Castrillo, G. Casa, A. Merlone, G. Galzerano, P. Laporta, L. Gianfrani, C.R. Physique **10**, 894 (2009)
223. C. Lemarchand, M. Triki, B. Darquié, Ch. J. Bordé, C. Chardonnet, C. Daussy, New J. Phys. **13**, 073028 (2011)
224. M.R. Moldover, J.P.M. Trusler, T.J. Edwards, J.B. Mehl, R.S. Davis, Phys. Rev. Lett. **60**, 249 (1988)
225. L.S. Rothman, I.E. Gordon, A. Barbe, D. Chris Benner, P.F. Bernath, M. Birk, V. Boudon, L.R. Brown, A. Campargue, J.-P. Champion, K. Chance, L.H. Coudert, V. Dana, V.M. Devi, S. Fally, J.-M. Flaud, R.R. Gamache, A. Goldman, D. Jacquemart, I. Kleiner, N. Lacome, W.J. Lafferty, J.-Y. Mandin, S.T. Massie, S.N. Mikhailenko, C.E. Miller, N. Moazzen-Ahmadi, O.V. Naumenko, A.V. Nikitin, J. Orphal, V.I. Perevalov, A. Perrin, A. Predoi-Cross, C.P. Rinsland, M. Rotger, M. Šimečková, M.A.H. Smith, K. Sung, S.A. Tashkun, J. Tennyson, R.A. Toth, A.C. Vandaele, J. Vander Auwera, J. Quant. Spectrosc. Radiat. Transf. **110**, 533 (2009)
226. N. Jacquinet-Husson, L. Crepeau, R. Armante, C. Boutammine, A. Chedin, N.A. Scott, C. Crevoisier, V. Capelle, C. Boone, N. Poulet-Crovisier, A. Barbe, A. Campargue, D. Chris Benner, Y. Benilan, B. Bezard, V. Boudon, L.R. Brown, L.H. Coudert, A. Coustenis, V. Dana, V.M. Devi, S. Fally, A. Fayt, J.-M. Flaud, A. Goldman, M. Herman, G.J. Harris, D. Jacquemart, A. Jolly, I. Kleiner, A. Kleinbohl, F. Kwabia-Tchana, N. Lavrentieva, N. Lacome, L.-H. Xu, O.M. Lyulin, J.-Y. Mandin, A. Maki, S. Mikhailenko, C.E. Miller, T. Mishina, N. Moazzen-Ahmadi, H.S.P. Muller, A. Nikitin, J. Orphal, V. Perevalov, A. Perrin, D.T. Petkie, A. Predoi-Cross, C.P. Rinsland, J.J. Remedios, M. Rotger, M.A.H. Smith, K. Sung, S. Tashkun, J. Tennyson, R.A. Toth, A.-C. Vandaele, J. Vander Auwera, JQSRT **112**, 2395 (2011)
227. S.-L. Cheah, Y.-P. Lee, J.F. Ogilvie, J. Quant. Spectrosc. Radiat. Transf. **64**, 467 (2000)

228. B. Lance, G. Blanquet, J. Walrand, J.-C. Populaire, J.-P. Bouanich, D. Robert, J. Molec. Spectrosc. **197**, 32 (1999)
229. A.S. Pine, T. Gabard, JQSRT **66**, 69 (2000)
230. J.W. Brault, L.R. Brown, C. Chackerian, R. Freedman, A. Predoi-Cross, A.S. Pine, J. Molec. Spectrosc. **222**, 220 (2003)
231. D. Lisak, G. Rusciano, A. Sasso, J. Mol. Spectrosc. **277**, 162 (2004)
232. D. Lisak, J.T. Hodges, Appl. Phys. B **88**, 317 (2007)
233. J.-P. Bouanich, G. Blanquet, J. Molec. Spectrosc. **241**, 186 (2007)
234. D.A. Shapiro, R. Ciuryło, R. Jaworski, A.D. May, Can. J. Phys. **79**, 1209 (2001)
235. H. Tran, J.-M. Hartmann, J. Chem. Phys. **130**, 094301 (2009)
236. D. Priem, J.-M. Colmont, F. Rohart, G. Wlodarczak, R.R. Gamache, J. Mol. Spectrosc. **204**, 204 (2000)
237. J.-M. Colmont, J.-F. D'Eu, F. Rohart, G. Wlodarczak, J. Buldyrevay, J. Mol. Spectrosc. **208**, 197 (2001)
238. M.A. Koshelev, M.Y. Tretyakov, F. Rohart, J.-P. Bouanich, J. Chem. Phys. **136**, 124316 (2012)
239. A. Predoi-Cross, F. Rohart, J.-P. Bouanich, D.R. Hurtmans, Can. J. Phys. **87**, 485 (2009)
240. G. Dufour, D. Hurtmans, A. Henry, A. Valentin, M. Lepere, J. Molec. Spectrosc. **221**, 80 (2003)